THE JOURNAL OF BIOLOGICAL CHEMISTRY VOL. 285, NO. 32, pp. 25044–25052, August 6, 2010

Structural and Kinetic Analysis of Free Methionine-*R*-sulfoxide Reductase from *Staphylococcus aureus*

CONFORMATIONAL CHANGES DURING CATALYSIS AND IMPLICATIONS FOR THE CATALYTIC AND INHIBITORY MECHANISMS[*] [S]

Received for publication, January 12, 2010, and in revised form, May 15, 2010 Published, JBC Papers in Press, May 25, 2010, DOI 10.1074/jbc.M110.103119

Seoung Min Bong[‡], Geun-Hee Kwak[§], Jin Ho Moon[¶], Ki Seog Lee[‖], Hong Seok Kim[**], Hwa-Young Kim[§1], and Young Min Chi[‡2]

*From the [‡]Division of Biotechnology, College of Life Sciences, and the [¶]Institute of Life Sciences and Natural Resources, Korea University, Seoul 136-713, Republic of Korea, the [§]Department of Biochemistry and Molecular Biology, Yeungnam University College of Medicine, Daegu 705-717, Republic of Korea, the [‖]Department of Clinical Laboratory Science, College of Health Science, Catholic University of Pusan, Pusan 609-757, Republic of Korea, and **Clinical Laboratory Science, Health Science Center at San Antonio, University of Texas, Austin, Texas 78229*

Free methionine-*R*-sulfoxide reductase (fRMsr) reduces free methionine *R*-sulfoxide back to methionine, but its catalytic mechanism is poorly understood. Here, we have determined the crystal structures of the reduced, substrate-bound, and oxidized forms of fRMsr from *Staphylococcus aureus*. Our structural and biochemical analyses suggest the catalytic mechanism of fRMsr in which Cys^{102} functions as the catalytic residue and Cys^{68} as the resolving Cys that forms a disulfide bond with Cys^{102}. Cys^{78}, previously thought to be a catalytic Cys, is a non-essential residue for catalytic function. Additionally, our structures provide insights into the enzyme-substrate interaction and the role of active site residues in substrate binding. Structural comparison reveals that conformational changes occur in the active site during catalysis, particularly in the loop of residues 97–106 containing the catalytic Cys^{102}. We have also crystallized a complex between fRMsr and isopropyl alcohol, which acts as a competitive inhibitor for the enzyme. This isopropyl alcohol-bound structure helps us to understand the inhibitory mechanism of fRMsr. Our structural and enzymatic analyses suggest that a branched methyl group in alcohol seems important for competitive inhibition of the fRMsr due to its ability to bind to the active site.

Reactive oxygen species can damage cellular components, including lipids, nucleic acids, and proteins. Damage to proteins by reactive oxygen species is probably due to oxidation of side chains of amino acid residues (1). The sulfur-containing amino acids, methionine and cysteine, are the most sensitive to oxidation. Oxidation of methionine generates a diastereomeric mixture of methionine *S*-sulfoxide (Met-*S*-O)[3] and methionine *R*-sulfoxide (Met-*R*-O) (2). Methionine oxidation is associated with a variety of physiological and pathological processes, such as cellular signaling, aging, and neurodegenerative diseases (3, 4). For example, methionine oxidation activates calcium/calmodulin-dependent protein kinase II in the absence of calcium (5), regulates the life span of yeast, fruit fly, and nematode (6–8), and may advance progression of Alzheimer and Parkinson diseases (9–12).

However, this oxidation can be reversed by the methionine-sulfoxide reductases (Msrs). Two distinct families of Msrs have evolved for the stereospecific reduction of methionine sulfoxides in proteins (13, 14). MsrA catalyzes the reduction of Met-*S*-O, whereas MsrB reduces Met-*R*-O. Most organisms from bacteria to humans possess a methionine sulfoxide reduction system that confers upon them the ability to repair oxidative damage and consequently impacts their longevity in oxidative environments (2, 4). In addition, Msrs are involved in the virulence mechanism of some bacterial pathogens, including *Mycoplasma genitalium* and *Neisseria gonorrhoeae* (15–17). Recently, an enzyme specific for the reduction of free Met-*R*-O has been identified from *Escherichia coli* and named fRMsr (18). This protein is found in unicellular organisms, including *Saccharomyces cerevisiae*, but absent in multicellular organisms (19). Interestingly, fRMsr contains a GAF domain, which is a ubiquitous motif present in cyclic GMP phosphodiesterases (20). Two variants of fRMsr proteins were detected with different conserved Cys residues (19); type I fRMsrs contain three conserved Cys residues, whereas type II fRMsrs have two.

The structures and catalytic mechanisms of MsrA and MsrB are well characterized (21–24). Although MsrA and MsrB are completely different in sequence and structure, they share a common catalytic mechanism involving formation of a sulfenic acid intermediate on the catalytic Cys, followed by regeneration

* This work was supported by a Korea University Grant 2009 (to Y. M. C.) and by Korea Healthcare Technology R&D Project (Ministry for Health, Welfare, and Family Affairs) Grant A090181 (to H. -Y. K.).

[S] The on-line version of this article (available at http://www.jbc.org) contains supplemental Figs. S1–S3.

The atomic coordinates and structure factors (codes 3KSF, 3KSG, 3KSH, and 3KSI) have been deposited in the Protein Data Bank, Research Collaboratory for Structural Bioinformatics, Rutgers University, New Brunswick, NJ (http://www.rcsb.org/).

[1] To whom correspondence may be addressed. Tel.: 82-53-620-4347; Fax: 82-53-654-6651; E-mail: hykim@ynu.ac.kr.

[2] To whom correspondence may be addressed. Tel.: 82-2-3290-3025; Fax: 82-2-921-3702; E-mail: ezeg@korea.ac.kr.

[3] The abbreviations used are: Met-*S*-O, methionine *S*-sulfoxide; Met-*R*-O, methionine *R*-sulfoxide; DTT, dithiothreitol; Msr, methionine-sulfoxide reductase; fRMsr, free methionine-*R*-sulfoxide reductase; Trx, thioredoxin; MES, 2-(*N*-morpholino)ethanesulfonic acid; DTT, dithiothreitol; r.m.s., root mean square; dabsyl, 4-(4-dimethylaminophenylazo)-benzolsulfonyl.

of the oxidized catalytic Cys. Briefly, a catalytic Cys attacks the sulfur of methionine sulfoxide and forms a sulfenic acid intermediate, with concomitant release of the product, methionine. The catalytic Cys sulfenic acid then forms an intramolecular disulfide bond by interacting with a resolving Cys. The disulfide bond is reduced by reductants, and consequently the enzyme becomes active again. Thioredoxin (Trx) is generally considered the *in vivo* reductant, whereas dithiothreitol (DTT) can be used *in vitro*. In contrast, the catalytic mechanism of fRMsr is poorly understood, although previous studies suggested that its catalytic mechanism is similar to those of MsrA and MsrB, involving the common sulfenic acid chemistry.

It has been found that *Staphylococcus aureus*, a leading cause of hospital- and community-acquired infections, contains a type I fRMsr, three MsrAs, and an MsrB (19, 25). *S. aureus* fRMsr contains three conserved Cys residues (Cys^{68}, Cys^{78}, and Cys^{102}). Two crystal structures of fRMsrs from *E. coli* and *S. cerevisae* are available (Protein Data Bank codes 1VHM (18, 26) and 1F5M (27), respectively). Both structures contain a disulfide bond between Cys^{68} and Cys^{102} (numbering is based on the *S. aureus* fRMsr) in the active sites, suggesting that fRMsrs use Cys residues for catalysis. The active site is enclosed in a small cavity (18, 19, 26, 27). This enclosed cavity supports the apparent substrate specificity for free Met-*R*-O but not for protein-based forms. Previous studies suggested that Cys^{78} functions as a catalytic residue, Cys^{102} as a primary resolving Cys, and Cys^{68} as a secondary resolving residue (18, 19). However, the roles of these three Cys residues are unclear in the catalysis of fRMsr. Thus, the catalytic mechanism of this enzyme has yet to be elucidated.

In this study, we resolved four structural forms of the *S. aureus* fRMsr by x-ray crystallography: reduced form ($fRMsr_{red}$), complexed form with the substrate ($fRMsr_{sub}$), oxidized form ($fRMsr_{ox}$), and another complexed form with isopropyl alcohol ($fRMsr_{isopro}$). The first three structures represent different catalytic states of fRMsr. The last structure, $fRMsr_{isopro}$, helps us to understand the inhibitory mechanism of fRMsr. We also performed biochemical analyses using the wild type *S. aureus* fRMsr and single and double mutants, in which the three conserved Cys are replaced with Ser. We studied the inhibitory effect of various alcohols on fRMsr. Our structural and enzymatic studies provide insights into the catalytic mechanism of fRMsr with conformational changes that occur during catalysis and into the inhibitory mechanism involving a branched methyl group of alcohols.

EXPERIMENTAL PROCEDURES

Purification, Crystallization, and X-ray Analysis—Gene cloning, protein expression, purification, and crystallization of *S. aureus* fRMsr have been described elsewhere for the oxidized and isopropyl alcohol-complexed forms of *S. aureus* fRMsr ($fRMsr_{ox}$ and $fRMsr_{isopro}$) (29). The crystal complexed with isopropyl alcohol was obtained from a crystallization solution consisting of 2 M ammonium sulfate and 10% (v/v) 2-propanol. For the reduced form of fRMsr ($fRMsr_{red}$), cell pellets were resuspended in ice-cold lysis buffer (20 mM Tris-HCl, pH 7.9, 500 mM NaCl, 5 mM imidazole, 10 mM β-mercaptoethanol, 1 mM phenylmethylsulfonyl fluoride). The purification procedures were similar to those of oxidized form, but 10 mM DTT was used in the final purification procedure of gel filtration. The crystallization condition comprised 24% polyethylene glycol 3350 and 0.35 M potassium fluoride. The substrate complex form of fRMsr ($fRMsr_{sub}$) was obtained by soaking 9 mM free Met-*R*-O in native crystals of mutant C68S fRMsr in which the crystallization condition comprised 26% polyethylene glycol 400 and 0.1 M MES, pH 6.4.

The crystals were soaked in a solution containing 25% (v/v) ethylene glycol used as cryoprotectant and frozen in liquid nitrogen. X-ray diffraction data were collected with an ADSC Quantum CCD 210 detector at beamlines 6C and 4A at Pohang Light Source (Pohang, South Korea). A total range of 360° was covered with 1.0° oscillation and 30-s exposure per frame. The crystal-to-detector distance was set to 150 mm. The data sets were processed and scaled using HKL 2000 (30). The $fRMsr_{red}$, $fRMsr_{sub}$, $fRMsr_{ox}$, and $fRMsr_{isopro}$ crystals diffracted to 1.9, 2.3, 1.5, and 1.7 Å, respectively. The detailed statistics are summarized in Table 1.

Model Building and Structure Refinement—The crystal structures of fRMsr were solved by molecular replacement methods using CNS (28) and Molrep (31) programs. The coordinates of *E. coli* fRMsr (Protein Data Bank code 1VHM) (18, 26) were used as the search model. Refinements were performed with several cycles of torsion-angle-simulated annealing, energy minimization, individual *B* factor refinement, and manual model rebuilding. The models were completed by iterative cycles of model building with Coot (32) and subsequently by refinement with CNS (28). The final models for $fRMsr_{red}$, $fRMsr_{sub}$, $fRMsr_{ox}$, and $fRMsr_{isopro}$ yielded R_{factor} and R_{free} values of 21.6 and 25.6% for $fRMsr_{red}$, 22.2 and 25.2% for $fRMsr_{sub}$, 22.1 and 23.4% for $fRMsr_{ox}$, and 22.0 and 24.2% for $fRMsr_{isopro}$, respectively. Refinement data were validated by the PROCHECK program (33) and are provided in Table 1. All figures were created using CCP4mg (34).

Measurements of Msr Activities—For free Msr activity, NADPH oxidation was monitored as a decrease of A_{340} at room temperature for 10 min in the reaction mixture. The reaction mixture (200 μl) contained 50 mM sodium phosphate (pH 7.5), 50 mM NaCl, 0.2 mM NADPH, 10 μg of *E. coli* Trx (Sigma), 14 μg of human Trx reductase 1, 0.1 mM EDTA, 1 mM free Met-*R*-O or free Met-*S*-O, and 2 or 10 μg of fRMsr enzyme. Enzyme activity was defined as nmol of oxidized NADPH/min using a molar extinction coefficient of 6220 M^{-1} cm^{-1}. K_m and V_{max} values were determined by non-linear regression using GraphPad Prism 5 software.

For peptide Msr activity, dabsylated methionine sulfoxide was used as the substrate in a DTT-dependent reaction. The reaction mixture (100 μl), containing 50 mM sodium phosphate (pH 7.5), 50 mM NaCl, 20 mM DTT, 200 μM dabsyl-Met-*R*-O or dabsyl-Met-*S*-O, and 1 μg of fRMsr enzyme, was incubated at 37 °C for 30 min. The reaction product, dabsyl-Met, was analyzed by high pressure liquid chromatography.

For inhibition assays of various alcohols on fRMsr activity, the reaction mixture (200 μl) contained 50 mM sodium phosphate (pH 7.5), 50 mM NaCl, 0.2 mM NADPH, 10 μg of *E. coli* Trx, 14 μg of human Trx reductase 1, 0.1 mM EDTA, 1 mM free Met-*R*-O, 1% various alcohols, and 2 μg of fRMsr enzyme. The

TABLE 1
Data collection statistics and refinement statistics

	$fRMsr_{red}$	$fRMsr_{sub}$	$fRMsr_{ox}$	$fRMsr_{isopro}$
Data collection				
Wavelength (Å)	1.23986	1.23986	1.23986	1.23986
Space group	$P2_1$	$P2_1$	$P6_122$	$P6_122$
Unit cell	$a = 69.0$	$a = 41.6$	$a = b = 90.0$	$a = b = 89.8$
	$b = 119.6$	$b = 87.5$	$c = 88.5$	$c = 88.8$
	$c = 80.3$	$c = 42.9$		
Resolution range (Å)	50.0–1.9 (1.93–1.9)[a]	50.0–2.3 (2.34–2.3)	50.0–1.5 (1.55–1.5)	50.0–1.7 (1.76–1.7)
Observed reflections	454,984	64,222	980,295	479,682
Unique reflections	98,600	13,036	33,994	23,645
Redundancy	4.6 (3.2)	4.9 (3.2)	28.9 (6.2)	20.3 (7.6)
Completeness (%)	98.1 (94.5)	97.5 (92.7)	98.6 (87.1)	99.1 (94.8)
R_{sym} (%)[b]	7.5 (33.6)	7.0 (23.6)	5.9 (33.0)	6.6 (28.7)
I/sigma (I)	19.2 (2.7)	13.4 (4.1)	14.5 (3.2)	16.0 (5.5)
Refinement statistics				
R_{factor}/R_{free} (%)	21.6/25.6	22.2/25.2	22.1/23.4	22.0/24.2
r.m.s. deviation bond (Å)	0.005	0.006	0.004	0.005
r.m.s. deviation angles (degrees)	1.2	1.2	1.1	1.2
Mean B factor	26.4	49.7	22.8	23.9
Ramachandran plot				
Most allowed region (%)	88.9	85.0	90.4	91.2
Additional allowed region (%)	10.9	12.0	9.6	8.8
Generously allowed region (%)	0.3	2.9	0	0
Disallowed region (%)	0	0	0	0

[a] Values in parentheses represent the highest resolution shell.
[b] $R_{sym} = \Sigma_{hkli}|I_{hkli} - \langle I_{hkl}\rangle|/\Sigma_{hkli} I_{hkli}$, where I is the observed intensity, $\langle I\rangle$ is the average intensity, and i is counts through all symmetry-related reflections. The crystallographic R_{factor} is based on 95% of the data used in refinement, and R_{free} is based on 5% of the data withheld for the cross-validation test.

reaction mixture was incubated at room temperature for 10 min, and the decrease of A_{340} was monitored.

Preparation of Single or Double Mutant Forms of S. aureus fRMsr—C68S, C78S, C102S, C68S/C78S, and C68S/C102S mutants were generated by site-directed mutagenesis using a pET28a-based wild type construct (29). All constructs were verified by DNA sequencing.

RESULTS AND DISCUSSION

Catalytic Activities of Wild Type and Mutant Forms of S. aureus fRMsr—First, we tested the substrate specificity of *S. aureus* fRMsr toward free Met-*R*-O, free Met-*S*-O, dabsyl-Met-*R*-O (mimic to peptide Met-*R*-O), dabsyl-Met-*S*-O, and dimethyl sulfoxide. The enzyme assay was performed by analyzing NADPH oxidation in the reaction mixture. As expected, *S. aureus* fRMsr reduced free Met-*R*-O but could not reduce free Met-*S*-O, dabsyl-Met-*R*-O, dabsyl-Met-*S*-O, or dimethyl sulfoxide, showing the same substrate specificity as *E. coli* and *S. cerevisiae* fRMsrs characterized previously (18, 19).

To determine the roles of the three conserved Cys residues (Cys^{68}, Cys^{78}, and Cys^{102}; supplemental Fig. S1) in catalysis, we mutated these residues to Ser, making single or double mutants (C68S, C78S, C102S, C68S/C78S, and C68S/C102S). We assayed the Trx-dependent activities of these mutant fRMsrs and compared them with the wild type. As shown in Table 2, the activity of C68S was 32% of wild type. Unexpectedly, the activity of C78S was 75% of wild type. This Cys residue was previously suggested to be the catalytic residue in *E. coli* and *S. cerevisae* fRMsrs (18, 19). Interestingly, C102S had no catalytic activity. Consistent with this result, C68S/C102S had no catalytic activity either, whereas C68S/C78S retained 22% of enzyme activity.

We then analyzed kinetic parameters of C78S, C68S, and C68S/C78S as well as wild type (Table 2). The V_{max} value of C78S was slightly higher than that of wild type; the K_m value was 2-fold higher than that of wild type. These data indicate that

TABLE 2
Specific activities and kinetic parameters of wild type and mutant forms of *S. aureus* fRMsr
Enzyme assays were performed using 10 μg of purified proteins as described under "Experimental Procedures." Values in parenthesis represent the activity relative to wild type. K_m and V_{max} values were determined by fitting the data to the Michaelis-Menten equation. NA, not assayed.

Proteins	Specific activity	K_m	V_{max}
	nmol/min/mg protein	μM	*nmol/min/mg protein*
Wild type	85 ± 5 (100)	50 ± 10	360 ± 10
C68S	27 ± 2 (32)	210 ± 20	280 ± 10
C78S	64 ± 20 (75)	110 ± 50	440 ± 50
C102S	0 ± 0.3 (0)	NA	NA
C68S/C78S	19 ± 3 (22)	830 ± 240	130 ± 20
C68S/C102S	0 ± 0.3 (0)	NA	NA

Cys^{78} is non-essential for catalysis by fRMsr. The V_{max} value was significantly reduced in C68S mutant, whereas the K_m value was 4-fold higher, compared with those of wild type. The double C68S/C78S mutant exhibited more decreased V_{max} (3-fold lower than wild type) and more increased K_m (16-fold higher than wild type).

Thus, in contrast to the previously suggested model, Cys^{102} is proposed to be the catalytic Cys, Cys^{68} may serve as the resolving Cys that forms a disulfide bond with Cys^{102}, and Cys^{78} is a non-essential residue for catalytic function. The above enzymatic data are consistent with our recent findings from *S. cerevisae* fRMsr that Cys^{125} (corresponding to Cys^{102} in *S. aureus* fRMsr) functions as the catalytic residue, as determined by enzyme and *in vivo* growth complementation assays (35).

Crystal Structure of the Reduced Form of fRMsr—Previously known structures from both *E. coli* and *S. cerevisae* fRMsrs are oxidized forms with a disulfide bond between Cys^{68} and Cys^{102} (26, 27). In addition, the *E. coli* fRMsr structure contains a complex with MES in the active site. Here, we resolved the structure of a reduced form of *S. aureus* fRMsr ($fRMsr_{red}$) (supplemental Fig. S2*A*). The crystal of $fRMsr_{red}$ comprises four dimers in the asymmetric unit. There are several hydrogen bond inter-

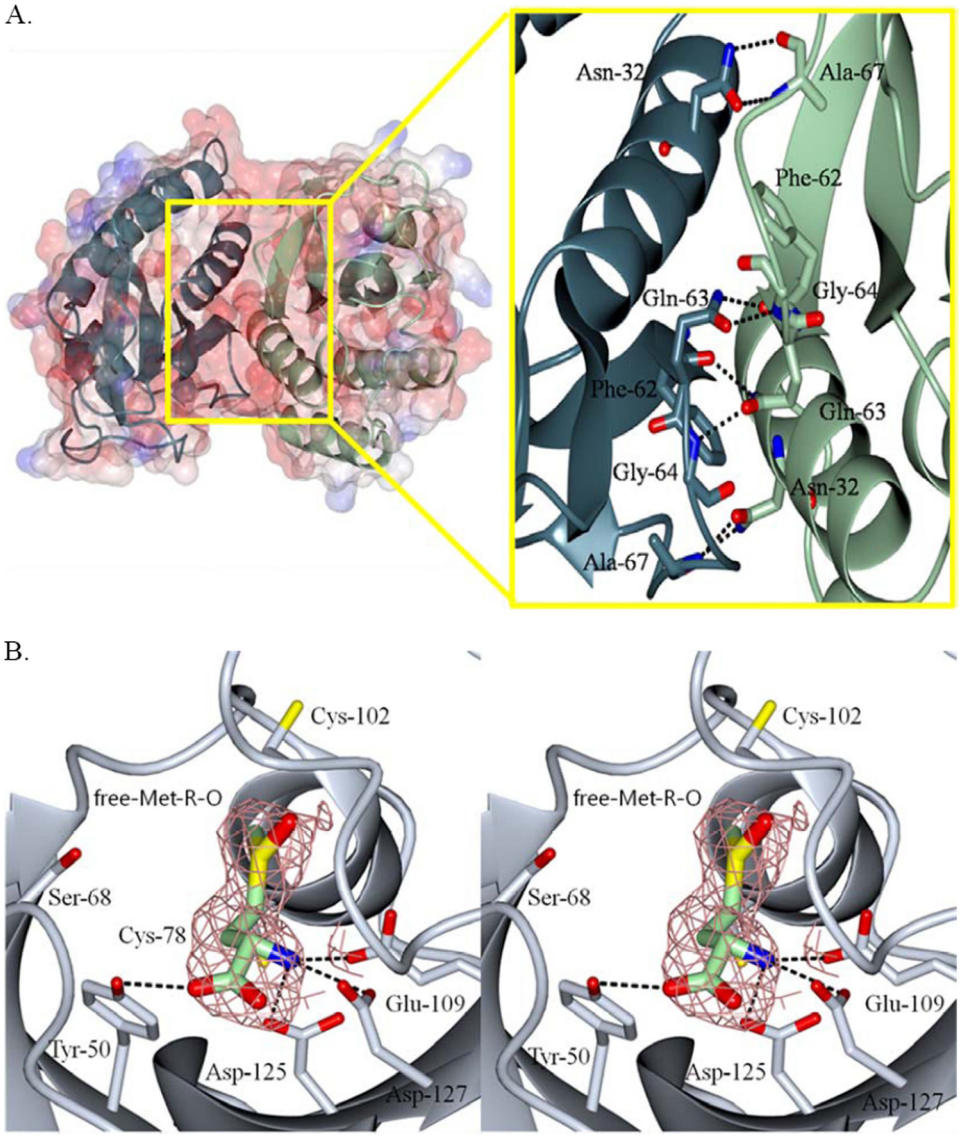

FIGURE 1. **The overall structure of a reduced form of *S. aureus* fRMsr (*A*) and structure of substrate-bound active site of C68S fRMsr in stereo (*B*).** In *A*, a dimer is shown by electrostatic surface and *ribbon models* (*blue*, C subunit; *light green*, D subunit). A *close-up view* represents the dimer interface region. In the interface region, Asn^{32}, Gln^{63}, Phe^{62}, and Ala^{67} of the C subunit interact by hydrogen-bonding, respectively, with Ala^{67}, Gly^{64}/Phe^{62}, Gln^{63}, and Asn^{32} of the other subunit. In *B*, the ligand, free Met-*R*-O, is depicted as a *light green stick model*. The omit electron density of substrate is shown at 1.5 σ. Hydrogen bond interactions between the substrate and the active site residues are indicated by *black dotted lines* (for details, see "Results and Discussion").

actions in the interface region of the dimer structure (Fig. 1*A*). To assess on quantitative grounds the possibility that these hydrogen bond interactions may stabilize an $fRMsr_{red}$ dimer, the dimer interface was evaluated by using the program PISA (36). This widely used program estimates a dimeric state for $fRMsr_{red}$ (complexation significance score = 1). In particular, this analysis shows that the buried area upon formation of the dimeric assembly is 932.7 $Å^2$, which accounts for 11.8% of the total surface area for each molecule. It should be noted that *S. cerevisae* fRMsr is also a dimer in solution (27).

The carboxamide groups of Asn^{32} and Gln^{63} from one subunit form hydrogen bonds with the backbones of Ala^{67} and Phe^{62} from the other subunit, respectively. In addition, the side chain of Gln^{63} of one subunit interacts with the backbone of Gly^{64} of the other subunit. The overall one-subunit structure of $fRMsr_{red}$ is composed of six antiparallel β-strands ($\beta1$–$\beta6$) and four α-helices ($\alpha1$–$\alpha4$) (supplemental Fig. S2*A*). The active site contained Trp^{46}, Tyr^{50}, Leu^{59}, Cys^{68}, Cys^{78}, Cys^{102}, Asp^{103}, Ala^{104}, Ser^{106}, Glu^{109}, Asp^{125}, and Asp^{127} in five antiparallel β-strands, two loops, and one α-helix, where Cys^{78} is located (Fig. 2*C* and supplemental Fig. S2*A*). The side chains of Cys^{102} and Cys^{68} are located in the active site. The distances between the sulfur atoms of Cys^{68} and Cys^{102}, Cys^{68} and Cys^{78}, and Cys^{78} and Cys^{102} are 5.7, 10.1, and 10.2 Å, respectively. On one side of the cavity of the active site, Trp^{46} and Ala^{104} form a hydrophobic region, whereas the opposite side displays a hydrophilic region consisting of Tyr^{50}, Glu^{109}, Asp^{125}, and Asp^{127}. The structure of $fRMsr_{red}$ contains several water molecules (Wat) in the active site. Particularly, Wat^{4} interacts with the side chains of Tyr^{50} (3.4 Å) and Asp^{125} (2.9 Å). Also, Wat^{104} interacts with the side chains of Glu^{109}, Asp^{125}, and Asp^{127}; Wat^{491} interacts with the side chain of Cys^{78}, Glu^{109}, and Asp^{125}, respectively (Fig. 2*C*). These interactions involving water molecules in the active site may stabilize the conformation of reduced fRMsr.

Structure of fRMsr in Complex with the Substrate—Here, we have resolved the first structure of *S. aureus* fRMsr complexed with the substrate free Met-*R*-O ($fRMsr_{sub}$) using C68S fRMsr, which shows a Michaelis-like complex (supplemental Fig. S2*B*). The sulfoxide moiety of the substrate was clearly shown in the omit electron density map of the active site (Fig. 1*B*). This structure could lead us to understand the catalytic mechanism of fRMsr, the mode of binding to the substrate, and the roles of the active site residues during catalysis. The structure of $fRMsr_{sub}$ comprises a dimer with the substrate in each subunit of the asymmetric unit. The overall conformation of $fRMsr_{sub}$, in which Ser replaces Cys^{68} in the loop of the active site, is conserved with the reduced form of wild type fRMsr (supplemental Fig. S2). However, there are significant conformational changes around the active site, as discussed below.

The substrate Met-*R*-O is positioned by several hydrogen bonds and stacking interactions. The acidic side chains of

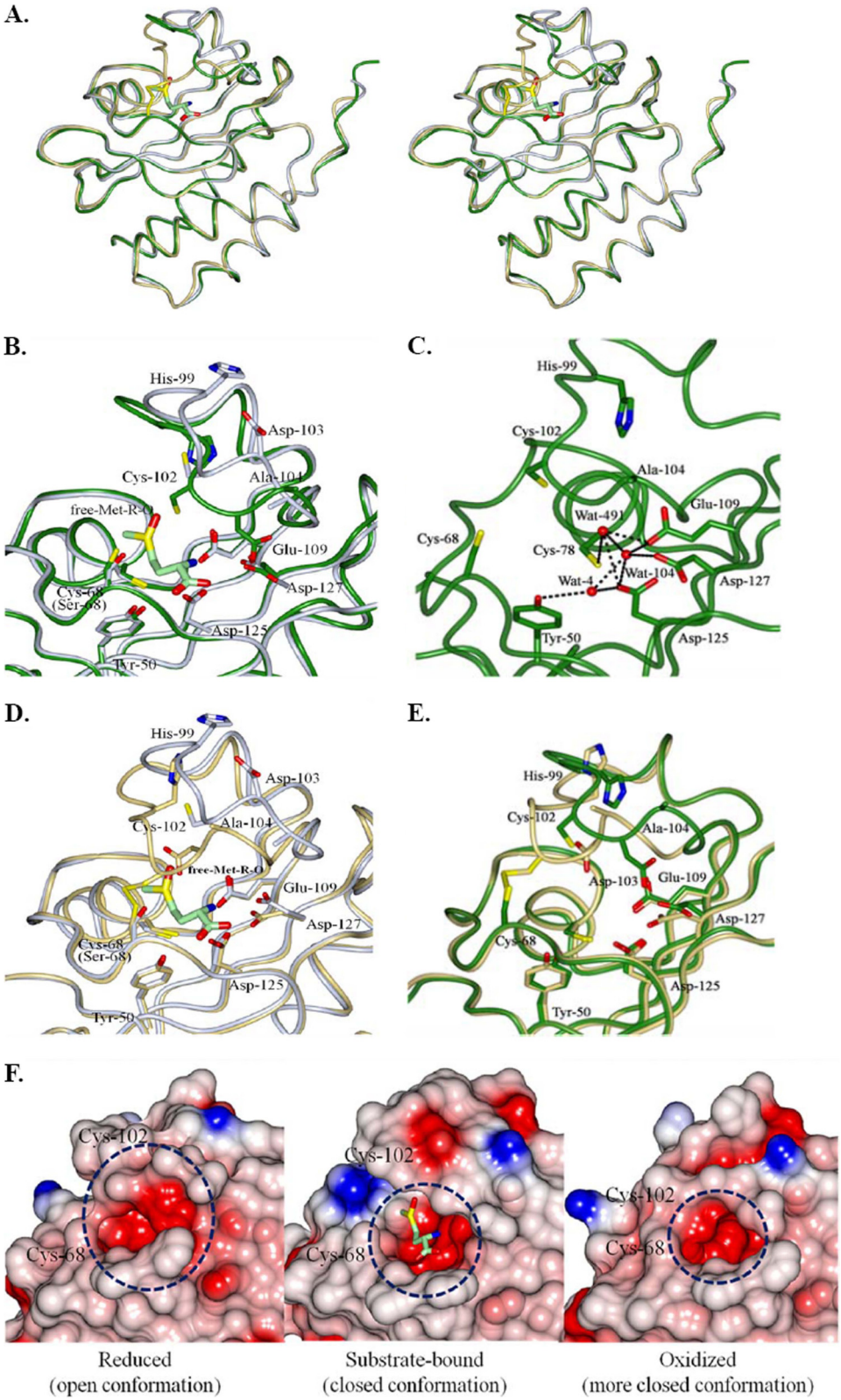

FIGURE 2. **Structural comparison of reduced, substrate-bound, and oxidized *S. aureus* fRMsrs.** *A*, stereoscopic views showing comparison of overall structures of reduced, substrate-bound, and oxidized *S. aureus* fRMsrs. The backbone models for reduced ($fRMsr_{red}$), substrate-bound ($fRMsr_{sub}$), and oxidized ($fRMsr_{ox}$) forms are shown in green, light blue, and light yellow, respectively. *B* and *C*, comparison of active sites between $fRMsr_{red}$ (*green*) and $fRMsr_{sub}$ (*light blue*). The active site residues of $fRMsr_{red}$ and $fRMsr_{sub}$ are superimposed (*B*), and those of $fRMsr_{red}$ are independently shown (*C*). In *C*, hydrogen bond interactions among water molecules and active site residues are indicated by *dotted lines*. *D*, comparison of active sites between $fRMsr_{sub}$ (*light blue*) and $fRMsr_{ox}$ (*light yellow*). The active site residues of $fRMsr_{sub}$ and $fRMsr_{ox}$ are superimposed. *E*, comparison of active sites between $fRMsr_{red}$ (*green*) and $fRMsr_{ox}$ (*light yellow*). The active site residues of $fRMsr_{red}$ and $fRMsr_{ox}$ are superimposed. The disulfide bond between Cys^{68} and Cys^{102} in $fRMsr_{ox}$ is represented by a *yellow stick*, and substrate Met-*R*-O in $fRMsr_{sub}$ is shown by a *light green stick*. *F*, conformational changes of $fRMsr_{red}$, $fRMsr_{sub}$, and $fRMsr_{ox}$. The active site is shown with electrostatic surface models. The surfaces are colored according to the electrostatic potentials from −21 kiloteslas/e (*red*) to +21 kiloteslas/e (*blue*). The electrostatic surface potentials were calculated by using APBS (37).

Glu^{109}, Asp^{125}, and Asp^{127} in the hydrophilic region form hydrogen bonds with nitrogen of the substrate (Fig. 1*B*). In addition, the residue Tyr^{50} forms a hydrogen bond with the carboxylate group of Met-*R*-O. The sulfoxide of the substrate is located close to Cys^{102}, pointing toward the sulfur atom of Cys^{102} (6.7 Å). The thiol of Cys^{78} points toward the carboxylate of the substrate although located closer to the sulfoxide of the substrate (4.3 Å). Our structural analysis, along with the above enzymatic data, suggests that Cys^{102} is the catalytic residue of fRMsr. The hydrophobic region involving Ala^{104} in the active site could accommodate the ϵ-methyl group of the substrate via van der Waals interactions, whereas the hydrophilic region could orient the substrate in the active site via hydrogen bonds with the nitrogen of the substrate. Also, this hydrophilic region may play a role in stabilizing the protonated oxygen atom of the sulfoxide moiety during catalysis. Thus, the hydrophobic pocket of the active site is shown to be essential for binding affinity to the substrate, whereas the hydrophilic region seems important for binding specificity.

Structure of the Oxidized Form of S. aureus fRMsr and a Comparison with Known fRMsr Structures—We also determined the structure of an oxidized form of *S. aureus* fRMsr (fRMsr$_{ox}$) containing a disulfide bond between Cys^{68} and Cys^{102} (supplemental Fig. S2*C*). The structure of fRMsr$_{ox}$ comprises one subunit in the asymmetric unit. However, fRMsr$_{ox}$ is found to form a dimer with a crystallographic 2-fold symmetry-related molecule in the unit cell. In fact, the fRMsr$_{red}$ and fRMsr$_{sub}$ structures were grown in the $p2_1$ monoclinic space group, whereas the fRMsr$_{ox}$ crystal grew in the $p6_122$ hexagonal space group.

We compared the *S. aureus* fRMsr$_{ox}$ with the structures of *E. coli* and *S. cerevisiae* fRMsrs previously reported, which are also oxidized forms with a disulfide bond between the above Cys residues. The oxidized *E. coli* fRMsr contains MES in the active site. *S. aureus* fRMsr shows 53% amino acid sequence identity with *E. coli* and *S. cerevisiae* fRMsrs, respectively (supplemental Fig. S1). The backbone structure of *S. aureus* fRMsr$_{ox}$ could be superimposed on the *E. coli* and *S. cerevisiae* fRMsrs with r.m.s. deviations of 1.6 and 5.4 Å, respectively, as determined by CNS (Crystallography and NMR System) (28) for 154 Cα atoms of the overall structures (supplemental Fig. S3*A*). Interestingly, there were significant differences in a loop region including the catalytic Cys^{102} (residues 97–106) between *S. aureus* fRMsr$_{ox}$ and *E. coli* fRMsr (supplemental Fig. S3*B*). Particularly, positions of His^{99}, Ala^{101}, and Asp^{103} move away from the corresponding residues of *E. coli* fRMsr to a distance of 3.3, 4.8, and 3.6 Å, respectively. Also, this loop region was significantly different from that of *S. cerevisiae* fRMsr (supplemental Fig. S3*C*). The positions of Ala^{101} and Asp^{103} move away from the corresponding residues of *S. cerevisiae* fRMsr to a distance of 4.2 and 6.1 Å, respectively. Thus, the structural comparison revealed that the catalytic Cys-containing loop region is quite flexible in fRMsr proteins.

Comparison and Conformational Changes of Reduced, Substrate-bound, and Oxidized Forms of fRMsr—We compared the reduced (fRMsr$_{red}$), substrate-bound (fRMsr$_{sub}$), and oxidized (fRMsr$_{ox}$) structures of *S. aureus* fRMsr (Fig. 2), which are representative of the catalytic steps of the fRMsr reaction.

The backbone structure of fRMsr$_{sub}$ could be superimposed on the fRMsr$_{red}$, with an r.m.s. deviation of 1.4 Å (Fig. 2*A*). There were significant conformational changes particularly in the loop consisting of residues 97–106 (Fig. 2*B*). Cys^{102} and Asp^{103} of fRMsr$_{sub}$ are the most displaced residues in the loop, shifted by 4.7 and 10.9 Å, respectively. The positions of Ile^{100}, His^{99}, and Lys^{97} lie at 2.4, 5.1, and 2.2 Å, respectively, from the corresponding residues of fRMsr$_{red}$. However, the position of Cys^{78} in fRMsr$_{sub}$ and fRMsr$_{red}$ remains relatively unchanged. The Glu^{109} residue in fRMsr$_{sub}$ resides at a distance of 3.6 Å from Asp^{127}, whereas in fRMsr$_{red}$ it resides at a distance of 4.7 Å. Cys^{68} and Cys^{102} residues in fRMsr$_{sub}$ reside at a distance of 9.7 and 11.7 Å, respectively, from Cys^{78}, whereas in fRMsr$_{red}$ they reside at a distance of 10.1 and 10.2 Å, respectively. Water molecules in the active site of fRMsr$_{red}$ interact with Glu^{109}, Asp^{125}, Asp^{127}, and Tyr^{50} residues that form hydrogen bonds with nitrogen and the carboxylate group of the substrate (Fig. 2*C*). When comparing the structure of fRMsr$_{sub}$ with fRMsr$_{red}$, the substrate Met-*R*-O in the active site replaces the water molecules occupied in the fRMsr$_{red}$ (Fig. 2, *B* and *C*).

We next compared the structure of fRMsr$_{sub}$ with fRMsr$_{ox}$. The backbone structure of fRMsr$_{sub}$ could be superimposed on the fRMsr$_{ox}$, with an r.m.s. deviation of 1.4 Å (Fig. 2*A*). Significant conformational changes are observed in the loop of residues 97–106 between these two structures (Fig. 2*D*). Cys^{102} and Asp^{103} residues are shifted by 6.7 and 7.8 Å, respectively, between fRMsr$_{sub}$ and fRMsr$_{ox}$. Specifically, in the substrate complex form, the loop moves into the active site compared with the oxidized form, resulting in positioning the thiol group of the catalytic Cys^{102} toward the entrance of the active site. The positions of Ile^{100}, His^{99}, and Gly^{98} in fRMsr$_{ox}$ lie at 6.6, 7.7, and 3.4 Å, respectively, from the corresponding residues of fRMsr$_{sub}$. However, the position of Cys^{78} in fRMsr$_{sub}$ and fRMsr$_{red}$ remains relatively unchanged.

We finally compared fRMsr$_{red}$ structure with fRMsr$_{ox}$ structure. The backbone structure of fRMsr$_{red}$ could be superimposed on the fRMsr$_{ox}$ with an r.m.s. deviation of 1.5 Å (Fig. 2*A*). Although the overall structures were well superimposed, there were significant differences in the loop of residues 94–106 (Fig. 2*E*). The loop in fRMsr$_{red}$ moves into the active site, which results in the positioning of the His^{99}, Cys^{102}, Asp^{103}, and Ala^{104} residues toward the entrance of active site. Large movements occur in the catalytic residue Cys^{102} and its neighboring residues Asp^{103} and Ala^{104}. The Cys^{102} residues in the oxidized and reduced forms of fRMsr reside at a distance of 4.7 Å from each other. Asp^{103} and Ala^{104} in the oxidized and reduced forms reside at a distance of 8.7 and 6.5 Å, respectively, from each other. The side chains of Glu^{109} and Asp^{127} in the active site reside farther from each other in fRMsr$_{red}$ (4.9 Å) than in fRMsr$_{ox}$ (3.7 Å). Moreover, the distance between Cys^{78} and Asp^{127} is changed from 5.8 Å in fRMsr$_{red}$ to 8.3 Å in fRMsr$_{ox}$. In addition, the fRMsr$_{red}$ structure shows movement of the side chain of Cys^{68} toward the entrance of the active site. Together, the movements of the active site residues (particularly Cys^{102}) determine the conformations of fRMsr$_{red}$ and fRMsr$_{ox}$, leading to an open conformation in fRMsr$_{red}$ and a closed conformation in fRMsr$_{ox}$ (Fig. 2*F*).

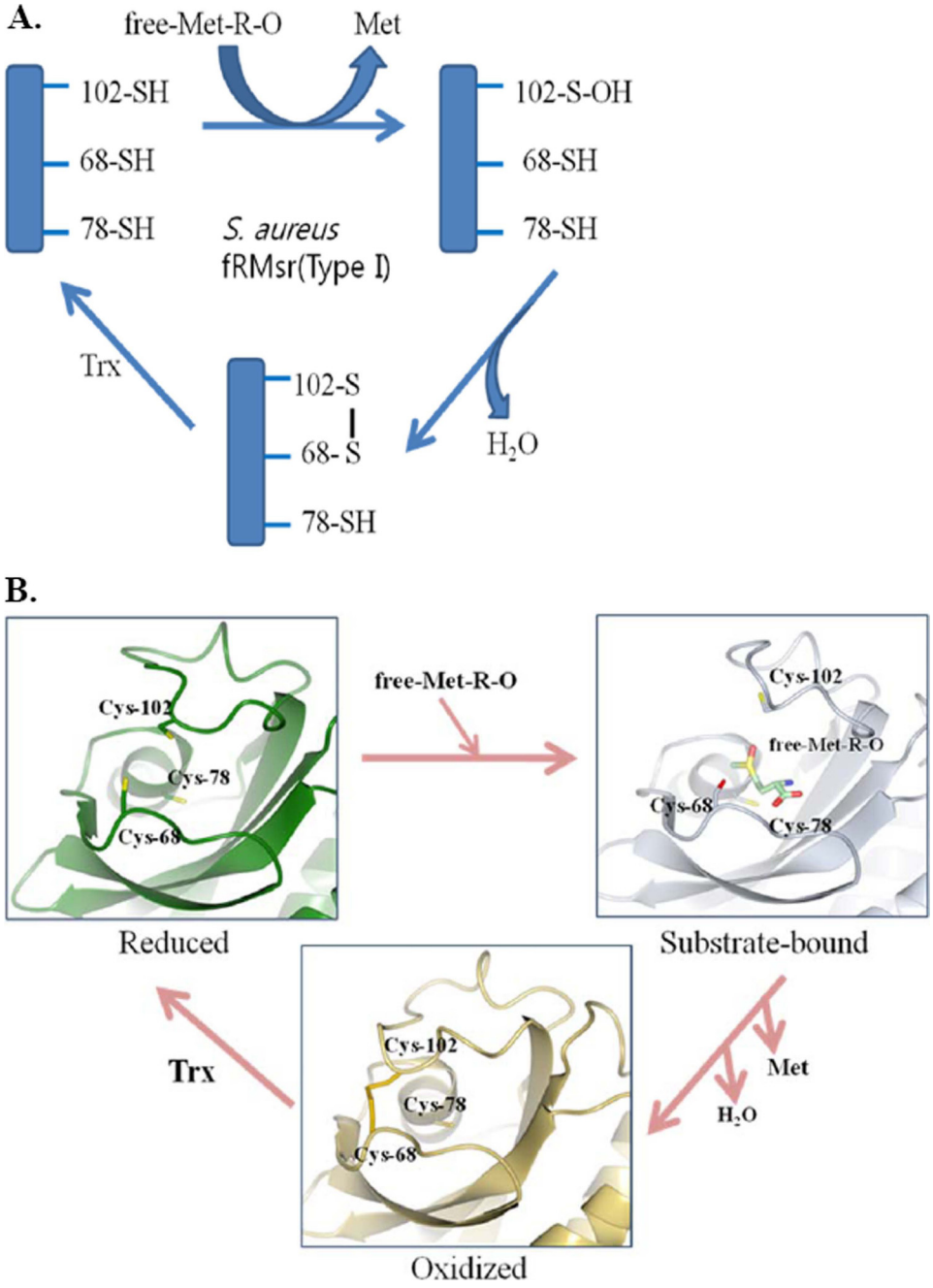

FIGURE 3. **Proposed catalytic mechanism of fRMsr.** *A*, a schematic representation. Catalytic Cys^{102} attacks free Met-*R*-O (*Met-R-O*) and is then oxidized to sulfenic acid. Cys^{68} acts as a resolving Cys and thus interacts with the Cys sulfenic acid to form a disulfide bond. The resulting Cys^{102}–Cys^{68} disulfide bond is reduced by a reductant (typically by Trx *in vivo* or by DTT *in vitro*), and finally the enzyme becomes active. Cys^{78} has no catalytic function. *B*, a structural representation. Reduced fRMsr initially displays an open conformation in the active site, and after binding of the substrate, the enzyme is converted to a closed conformation. Formation of a disulfide bond between Cys^{102} and Cys^{68} makes the enzyme more closed.

Catalytic Mechanism—Our crystal structures of $fRMsr_{red}$, $fRMsr_{sub}$, and $fRMsr_{ox}$ help in understanding the mode of binding of the substrate Met-*R*-O to the active site of fRMsr, the roles of the active site residues, and the conformational changes of fRMsr during catalysis. Significant conformational changes of the active site, particularly in the loop including the catalytic Cys, occur in each catalytic step. The reduced form has an open conformation to allow access to the substrate, the substrate-bound form takes a closed conformation after accommodation of Met-*R*-O, and the oxidized form is turned to a more closed conformation after catalysis (Fig. 2*F*).

Among the three conserved Cys residues, Cys^{102} was the most mobile, whereas Cys^{78}, the previously suggested catalytic residue from *E. coli* and *S. cerevisiae* fRMsrs (18, 19), was the most immobile. Our enzymatic studies concluded that Cys^{102} is the catalytic residue. Cys^{68} is suggested to be the resolving Cys by structural and kinetic analyses. Cys^{78} had no catalytic function, but this residue may play a role in substrate binding, as judged by the kinetic data (*i.e.* an increase in K_m value in the C78S mutant). Here, we propose that the catalytic mechanism of fRMsr consists of three steps. 1) Cys^{102} attacks the sulfoxide moiety of Met-*R*-O and is then oxidized to Cys sulfenic acid. 2) Cys^{68} interacts with the sulfenic acid intermediate to form a disulfide bond. 3) Finally, the Cys^{102}–Cys^{68} disulfide bond is reduced by a reductant (typically by Trx), and the fRMsr enzyme activity is regenerated (Fig. 3).

It should be noted that, in contrast to type I fRMsrs, type II enzymes contain only the conserved Cys^{78} and Cys^{102}. They lack Cys^{68}. Because our studies revealed no direct function for Cys^{78} in the catalysis of type I fRMsr, it is questionable whether this residue plays any role in the catalysis of type II fRMsr. It is possible that this Cys^{78} would function as a resolving Cys, replacing the role of Cys^{68} in type I enzymes. Thus, biochemical and structural studies of type II fRMsr would be interesting.

Implications of the Mechanism of Action of fRMsr Using a Competitive Inhibitor—We determined another complex structure ($fRMsr_{isopro}$) that contains isopropyl alcohol in the active site pocket of fRMsr. This crystal was obtained from a crystallization solution consisting of 2 M ammonium sulfate and 10% (v/v) isopropyl alcohol and had one subunit of protein in the asymmetric unit like $fRMsr_{ox}$. The $fRMsr_{isopro}$ structure also contains a disulfide bond formed by Cys^{68} and Cys^{102}. Interestingly, the binding pattern of isopropyl alcohol is expected to define the location of the substrate binding site (Fig. 4). The hydroxyl group of isopropyl alcohol interacts by hydrogen-bonding with Glu^{109},

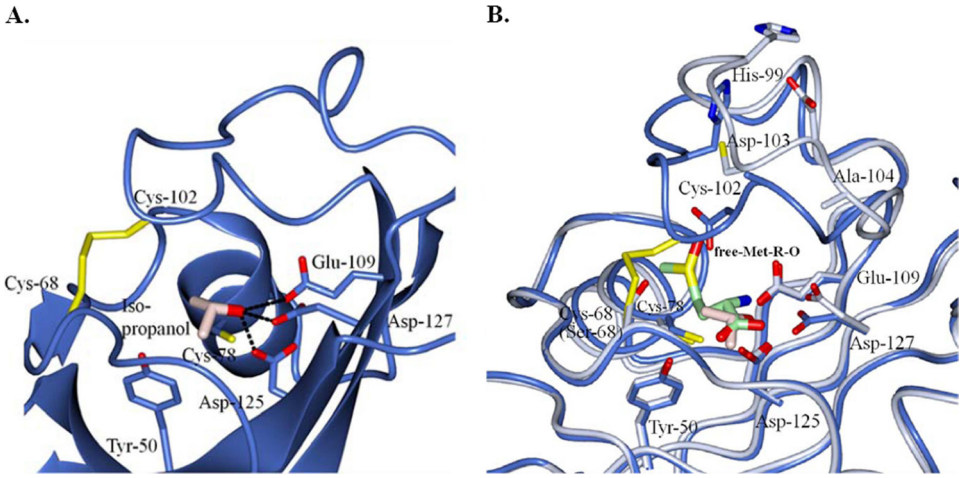

FIGURE 4. **Structure of isopropyl alcohol-bound *S. aureus* fRMsr and its comparison with the substrate-bound form.** *A*, the active site of $fRMsr_{isopro}$. Interactions between isopropyl alcohol (*Iso-propanol*) and active site residues are represented by *dotted lines*. *B*, comparison of active sites between $fRMsr_{isopro}$ (*light blue*) and $fRMsr_{sub}$ (*light gray*). The active site residues of $fRMsr_{isopro}$ and $fRMsr_{sub}$ are superimposed. Disulfide bonds between Cys^{68} and Cys^{102} and isopropyl alcohol in $fRMsr_{isopro}$ are shown by *yellow* and *light pink sticks*, respectively, and substrate Met-*R*-O (*Met-R-O*) in $fRMsr_{sub}$ is shown by a *light green stick*.

TABLE 3

Relative activity of fRMsr enzyme with various alcohols

Enzyme assays were performed in the presence of 1% various alcohols as described under "Experimental Procedures."

Alcohol	Relative activity
	%
None	100
Ethanol	91
n-Propyl alcohol	91
Isopropyl alcohol	69
n-Butyl alcohol	87
Isobutyl alcohol	52

Asp^{125}, and Asp^{127}, respectively. This is similar to the hydrogen bond interactions of these residues with the nitrogen of the substrate in $fRMsr_{sub}$. This structural analysis suggests that isopropyl alcohol could act as a competitive inhibitor of fRMsr enzyme. To test this hypothesis, we assayed the enzyme activities in the presence of 1% ethanol, *n*-propyl alcohol, or isopropyl alcohol (Table 3). Relative activities of fRMsr in the presence of ethanol and *n*-propyl alcohol were 91%. However, in the presence of isopropyl alcohol, the enzyme activity significantly decreased to 69%. We further determined kinetic parameters in the presence of 1% isopropyl alcohol. The K_m value was 100 ± 30 μM, which is 2-fold higher than that in the absence of isopropyl alcohol. The V_{max} value was 420 ± 30 nmol/min/mg of protein, similar to that without isopropyl alcohol. These results indicated that isopropyl alcohol can competitively inhibit fRMsr activity. Moreover, a branched methyl group in isopropyl alcohol may play a role in this inhibitory effect.

We further tested the inhibitory effect with 1% *n*-butyl alcohol and isobutyl alcohol (Table 3). In the presence of *n*-butyl alcohol, the relative activity was 87%, similar to that with ethanol or *n*-propyl alcohol. However, the enzyme activity was significantly inhibited by 50% in the presence of isobutyl alcohol. Together, our results indicate that a branched methyl group in alcohols seems important for competitive inhibition of fRMsr enzyme activity. The branched methyl group of alcohols may be crucial for binding to the active site in order to competitively inhibit the fRMsr activity, suggesting that the methyl group of the substrate may be important for binding affinity to the enzyme shown in the structure of $fRMsr_{sub}$.

In summary, we have determined the crystal structures of reduced, substrate-bound, oxidized, and inhibitor-bound fRMsrs at atomic resolution levels. Our structural and biochemical studies suggest the catalytic mechanism of fRMsr, where Cys^{102} acts as the catalytic residue and Cys^{68} acts as the resolving Cys. Our structures show the mode of binding of the substrate free Met-*R*-O, the roles of active site residues in catalysis, and the conformational changes of the active site during catalysis, particularly by the loop containing the catalytic Cys^{102}. In addition, our studies with a competitive inhibitor, isopropyl alcohol, predict the mechanism of action of fRMsr, where the methyl group in the substrate or a branched methyl group in alcohols seems important for interaction with the enzyme.

Acknowledgments—We thank the staff for assistance during the data collection at beamlines 6C and 4A of Pohang Light Source, South Korea.

REFERENCES

1. Stadtman, E. R. (2006) *Free Radic. Res.* **40,** 1250–1258
2. Weissbach, H., Resnick, L., and Brot, N. (2005) *Biochim. Biophys. Acta* **1703,** 203–212
3. Kim, H. Y., and Gladyshev, V. N. (2007) *Biochem. J.* **407,** 321–329
4. Moskovitz, J. (2005) *Biochim. Biophys. Acta* **1703,** 213–219
5. Erickson, J. R., Joiner, M. L., Guan, X., Kutschke, W., Yang, J., Oddis, C. V., Bartlett, R. K., Lowe, J. S., O'Donnell, S. E., Aykin-Burns, N., Zimmerman, M. C., Zimmerman, K., Ham, A. J., Weiss, R. M., Spitz, D. R., Shea, M. A., Colbran, R. J., Mohler, P. J., and Anderson, M. E. (2008) *Cell* **133,** 462–474
6. Koc, A., Gasch, A. P., Rutherford, J. C., Kim, H. Y., and Gladyshev, V. N. (2004) *Proc. Natl. Acad. Sci. U.S.A.* **101,** 7999–8004
7. Minniti, A. N., Cataldo, R., Trigo, C., Vasquez, L., Mujica, P., Leighton, F., Inestrosa, N. C., and Aldunate, R. (2009) *Aging Cell* **8,** 690–705
8. Ruan, H., Tang, X. D., Chen, M. L., Joiner, M. L., Sun, G., Brot, N., Weissbach, H., Heinemann, S. H., Iverson, L., Wu, C. F., Hoshi, T., Chen, M. L., Joiner, M. A., and Heinemann, S. H. (2002) *Proc. Natl. Acad. Sci. U.S.A.* **99,** 2748–2753
9. Barnham, K. J., Ciccotosto, G. D., Tickler, A. K., Ali, F. E., Smith, D. G., Williamson, N. A., Lam, Y. H., Carrington, D., Tew, D., Kocak, G., Volitakis, I., Separovic, F., Barrow, C. J., Wade, J. D., Masters, C. L., Cherny, R. A., Curtain, C. C., Bush, A. I., and Cappai, R. (2003) *J. Biol. Chem.* **278,** 42959–42965
10. Hou, L., Kang, I., Marchant, R. E., and Zagorski, M. G. (2002) *J. Biol. Chem.* **277,** 40173–40176
11. Schöneich, C. (2005) *Biochim. Biophys. Acta* **1703,** 111–119
12. Wassef, R., Haenold, R., Hansel, A., Brot, N., Heinemann, S. H., and Hoshi, T. (2007) *J. Neurosci.* **27,** 12808–12816

13. Lee, B. C., Dikiy, A., Kim, H. Y., and Gladyshev, V. N. (2009) *Biochim. Biophys. Acta* **1790,** 1471–1477
14. Weissbach, H., Etienne, F., Hoshi, T., Heinemann, S. H., Lowther, W. T., Matthews, B., St. John, G., Nathan, C., and Brot, N. (2002) *Arch. Biochem. Biophys.* **397,** 172–178
15. Dhandayuthapani, S., Blaylock, M. W., Bebear, C. M., Rasmussen, W. G., and Baseman, J. B. (2001) *J. Bacteriol.* **183,** 5645–5650
16. Olry, A., Boschi-Muller, S., Marraud, M., Sanglier-Cianferani, S., Van Dorsselear, A., and Branlant, G. (2002) *J. Biol. Chem.* **277,** 12016–12022
17. Sasindran, S. J., Saikolappan, S., and Dhandayuthapani, S. (2007) *Future Microbiol.* **2,** 619–630
18. Lin, Z., Johnson, L. C., Weissbach, H., Brot, N., Lively, M. O., and Lowther, W. T. (2007) *Proc. Natl. Acad. Sci. U.S.A.* **104,** 9597–9602
19. Le, D. T., Lee, B. C., Marino, S. M., Zhang, Y., Fomenko, D. E., Kaya, A., Hacioglu, E., Kwak, G. H., Koc, A., Kim, H. Y., and Gladyshev, V. N. (2009) *J. Biol. Chem.* **284,** 4354–4364
20. Zoraghi, R., Corbin, J. D., and Francis, S. H. (2004) *Mol. Pharmacol.* **65,** 267–278
21. Boschi-Muller, S., Gand, A., and Branlant, G. (2008) *Arch. Biochem. Biophys.* **474,** 266–273
22. Kim, Y. K., Shin, Y. J., Lee, W. H., Kim, H. Y., and Hwang, K. Y. (2009) *Mol. Microbiol.* **72,** 699–709
23. Lowther, W. T., Weissbach, H., Etienne, F., Brot, N., and Matthews, B. W. (2002) *Nat. Struct. Biol.* **9,** 348–352
24. Tête-Favier, F., Cobessi, D., Boschi-Muller, S., Azza, S., Branlant, G., and Aubry, A. (2000) *Structure* **8,** 1167–1178
25. Singh, V. K., and Moskovitz, J. (2003) *Microbiology* **149,** 2739–2747
26. Badger, J., Sauder, J. M., Adams, J. M., Antonysamy, S., Bain, K., Bergseid, M. G., Buchanan, S. G., Buchanan, M. D., Batiyenko, Y., Christopher, J. A., Emtage, S., Eroshkina, A., Feil, I., Furlong, E. B., Gajiwala, K. S., Gao, X., He, D., Hendle, J., Huber, A., Hoda, K., Kearins, P., Kissinger, C., Laubert, B., Lewis, H. A., Lin, J., Loomis, K., Lorimer, D., Louie, G., Maletic, M., Marsh, C. D., Miller, I., Molinari, J., Muller-Dieckmann, H. J., Newman, J. M., Noland, B. W., Pagarigan, B., Park, F., Peat, T. S., Post, K. W., Radojicic, S., Ramos, A., Romero, R., Rutter, M. E., Sanderson, W. E., Schwinn, K. D., Tresser, J., Winhoven, J., Wright, T. A., Wu, L., Xu, J., and Harris, T. J. (2005) *Proteins* **60,** 787–796
27. Ho, Y. S., Burden, L. M., and Hurley, J. H. (2000) *EMBO J.* **19,** 5288–5299
28. Brünger, A. T., Adams, P. D., Clore, G. M., DeLano, W. L., Gros, P., Grosse-Kunstleve, R. W., Jiang, J. S., Kuszewski, J., Nilges, M., Pannu, N. S., Read, R. J., Rice, L. M., Simonson, T., and Warren, G. L. (1998) *Acta Crystallogr. D* **54,** 905–921
29. Bong, S. M., Moon, J. H., Kim, H. Y., Kim, H. S., Kim, A. Y., and Chi, Y. M. (2009) *Acta Crystallogr. F* **65,** 1120–1122
30. Otwinowski, Z., and Minor, W. (1997) *Methods Enzymol.* **276,** 307–326
31. Vagin, A., and Teplyakov, A. (1997) *J. Appl. Crystallogr.* **30,** 1022–1025
32. Emsley, P., and Cowtan, K. (2004) *Acta Crystallogr. D* **60,** 2126–2132
33. Laskowski, R. A., MacArthur, M. W., Moss, D. S., and Thornton, J. M. (1996) *J. Appl. Crystallogr.* **26,** 283–291
34. Potterton, L., McNicholas, S., Krissinel, E., Gruber, J., Cowtan, K., Emsley, P., Murshudov, G. N., Cohen, S., Perrakis, A., and Noble, M. (2004) *Acta Crystallogr. D* **60,** 2288–2294
35. Kwak, G. H., Kim, M. J., and Kim, H. Y. (2010) *Biochem. Biophys. Res. Commun.* **395,** 412–415
36. Krissinel, E., and Henrick, K. (2007) *J. Mol. Biol.* **372,** 774–797
37. Baker, N. A., Sept, D., Joseph, S., Holst, M. J., and McCammon, J. A. (2001) *Proc. Natl. Acad. Sci. U.S.A.* **98,** 10037–10041